HETEROGENEOUS INFORMATION FUSION FOR MULTITARGET TRACKING USING THE SUM-PRODUCT ALGORITHM

Giovanni Soldi[†], Domenico Gaglione[†], Florian Meyer[‡], Franz Hlawatsch[*], Paolo Braca[†], Alfonso Farina[**], and Moe Z. Win[‡]

[†]NATO STO-CMRE, La Spezia, Italy (e-mail: [giovanni.soldi, domenico.gaglione, paolo.braca]@cmre.nato.int)
[‡]Laboratory for Information and Decision Systems, MIT, Cambridge, MA, USA (e-mail: [fmeyer, win]@mit.edu)
[*]Institute of Telecommunications, TU Wien, Vienna, Austria (e-mail: franz.hlawatsch@tuwien.ac.at)
[**]Professional Consultant, Rome, Italy (e-mail: alfonso.farina@outlook.it)

ABSTRACT

The sum-product algorithm (SPA) was recently shown to provide a scalable methodology for multitarget tracking (MTT) using multiple sensors. Here, we focus on another advantage of the SPA framework, namely, its capacity for Bayesian fusion of heterogeneous data sources and auxiliary information. We develop extensions of the SPA-based multisensor MTT algorithm that integrate data from an auxiliary surveillance system and geographic information about standard target routes. The effectiveness of our approach is demonstrated for a simulated scenario and for a real maritime scenario.

***Index Terms*—** Multitarget tracking, factor graph, sum-product algorithm, probabilistic data association, information fusion.

1. INTRODUCTION

Multitarget tracking (MTT) [1–12] aims at estimating the number and states of multiple targets from measurements provided by one or multiple sensors. The difficulty and complexity of MTT are mostly due to the measurement origin uncertainty (MOU) [1], i.e., the fact that it is not known from which target, if any, a given measurement originated. Recently, a Bayesian message passing algorithm for MTT that efficiently resolves the MOU problem was presented in [3,4]. This algorithm uses the sum-product algorithm (SPA) [13] for efficient approximate marginalizations of the joint posterior probability density function (pdf) of the target states.

In addition to improved scalability as discussed in [3–5], the SPA-based MTT algorithm enables an efficient and effective Bayesian fusion of heterogeneous sensors and other data sources. In this paper, we consider the integration of information provided by an auxiliary surveillance system such as the automatic identification system (AIS) [14] and of geographic information about standard target routes, such as sea lanes in a maritime environment [15]. This integration is achieved by the formal inclusion of an additional sensor in the first case and by the introduction of multiple dynamic models in the second case. The remainder of this paper is organized as follows. The SPA-based MTT algorithm for multiple radar sensors [3, 4] is briefly reviewed in Section 2, where also an adaptive extension supporting multiple dynamic models [16] is described. In Sections 3 and 4, we discuss the integration of, respectively, data provided by an auxiliary surveillance system and geographic information about standard target routes. In Sections 5 and 6, the performance of the algorithm proposed in Section 3 is assessed in a simulated scenario and in a real maritime scenario, respectively.

This work was supported in part by the NATO Allied Command Transformation under project SAC000808, by the European Research Council (ERC) under grant 700478 (project RANGER) within the Horizon 2020 program, by the Austrian Science Fund (FWF) under grants J3886-N31, P27370-N30, and P32055-N31, by the DARPA under US Navy Contract N66001-19-C-4004, by the MIT Institute for Soldier Nanotechnologies, and by the Czech Science Foundation (GAČR) under grant 17-19638S.

2. SPA-BASED MULTISENSOR MTT ALGORITHM

This section reviews the SPA-based multisensor MTT algorithm [3, 4] and its extension to multiple dynamic models [16].

2.1. System Model

While the number of targets is unknown, we fix the maximum possible number of targets, n_{t}. Accordingly, we consider n_{t} *potential targets* (PTs) $k \in \mathcal{K} \triangleq \{1, 2, \ldots, n_{\mathrm{t}}\}$ [3,4]. The existence of PT k at a given (current) time step is described by $r_k \in \{0, 1\}$ in the sense that PT k exists (does not exist) if r_k is 1 (0). The state of PT k at the current time step is denoted as $\boldsymbol{x}_k$; it consists of the PT's position and possibly further parameters, and is formally considered also if $r_k = 0$. The vector $\boldsymbol{y}_k \triangleq [\boldsymbol{x}_k^{\mathrm{T}} \; r_k]^{\mathrm{T}}$ will be termed the *augmented state* of PT k. We also denote by $\boldsymbol{y}_k^- \triangleq [\boldsymbol{x}_k^{-\mathrm{T}} \; r_k^-]^{\mathrm{T}}$ the augmented state of PT k at the previous time step, and by $\boldsymbol{y}$ and $\boldsymbol{y}^-$ the vectors stacking all the augmented PT states at the current time step and at the previous time step, respectively. The temporal evolution of the kth PT state is described by the state-transition pdf $f(\boldsymbol{x}_k|\boldsymbol{x}_k^-)$. This is embedded in the augmented state-transition pdf $f(\boldsymbol{y}_k|\boldsymbol{y}_k^-)$, which also models the birth/death of PT k [4].

There are n_{s} sensors $s \in \{1, 2, \ldots, n_{\mathrm{s}}\}$ that produce measurements $\boldsymbol{z}_m^{(s)}$ resulting from the detection stage of the radar signal processing chain [17]. An existing PT k (i.e., with $r_k = 1$) is "detected" by sensor s—in the sense that it generates a measurement $\boldsymbol{z}_m^{(s)}$ at sensor s—with probability $q^{(s)}$. Let $\mathcal{M}^{(s)} \triangleq \{1, 2, \ldots, n_{\mathrm{m}}^{(s)}\}$ comprise the indices m of the measurements $\boldsymbol{z}_m^{(s)}$ produced by sensor s at the current time. A measurement $\boldsymbol{z}_m^{(s)}$ generated by an existing PT k is modeled by the likelihood function $f\big(\boldsymbol{z}_m^{(s)}\big|\boldsymbol{x}_k\big)$. We denote by $\boldsymbol{z}^{(s)}$ the vector of all the $\boldsymbol{z}_m^{(s)}$, $m \in \mathcal{M}^{(s)}$, and by $\boldsymbol{z}$ and $\boldsymbol{z}^-$ the vectors of all the measurements of all the sensors up to the current time step and up to the previous time step, respectively.

The association between the measurements and the existing PTs is generally unknown, and it is also possible that a measurement did not originate from any PT (false alarm) or that a PT did not generate any measurement (missed detection). This uncertainty is referred to as MOU. We make the assumption—hereafter referred to as data association assumption—that an existing PT can generate at most one measurement at a given sensor and a measurement can originate from at most one existing PT [1]. Let us define the *PT-oriented*

association variable $a_k^{(s)}$, $k \in \mathcal{K}$ to be $m \in \mathcal{M}^{(s)}$ if PT k generates measurement m at sensor s, and zero if PT k is missed by sensor s. Similarly, we define the *measurement-oriented association variable* $b_m^{(s)}$, $m \in \mathcal{M}^{(s)}$ to be $k \in \mathcal{K}$ if measurement m at sensor s originates from PT k, and zero if it is a false alarm. Finally, following [5], we define the indicator function $\Psi_{km}^{(s)}\big(a_k^{(s)}, b_m^{(s)}\big)$ to be one if the values of $a_k^{(s)}$ and $b_m^{(s)}$ are consistent and zero otherwise. More formally, $\Psi_{km}^{(s)}\big(a_k^{(s)}, b_m^{(s)}\big) = 0$ if and only if either $a_k^{(s)} = m$ and $b_m^{(s)} \neq k$ or $a_k^{(s)} \neq m$ and $b_m^{(s)} = k$. We also denote by $\boldsymbol{a}$ and $\boldsymbol{b}$ the vectors of, respectively, all the $a_k^{(s)}$, $k \in \mathcal{K}$ and all the $b_m^{(s)}$, $m \in \mathcal{M}^{(s)}$ for all the sensors at the current time step.

2.2. Target Detection and State Estimation

The ultimate goal of MTT is to determine if a PT $k \in \mathcal{K}$ exists and to estimate the states $\boldsymbol{x}_k$ of the detected PTs. In the Bayesian setting, this essentially amounts to calculating the posterior existence probabilities $p(r_k = 1|\boldsymbol{z})$ and the posterior state pdfs $f(\boldsymbol{x}_k|r_k = 1, \boldsymbol{z})$. PT k is detected—i.e., declared to exist—if $p(r_k = 1|\boldsymbol{z})$ is larger than a suitably chosen threshold P_{th} [18, Ch. 2]. Then, for each detected PT k, an estimate of $\boldsymbol{x}_k$ is provided by, e.g., the minimum mean-square error estimator $\hat{\boldsymbol{x}}_k \triangleq \int \boldsymbol{x}_k f(\boldsymbol{x}_k|r_k = 1, \boldsymbol{z}) \mathrm{d}\boldsymbol{x}_k$ [18, Ch. 4]. The statistics $p(r_k = 1|\boldsymbol{z})$ and $f(\boldsymbol{x}_k|r_k = 1, \boldsymbol{z})$ can be obtained from the posterior pdf $f(\boldsymbol{x}_k, r_k|\boldsymbol{z}) = f(\boldsymbol{y}_k|\boldsymbol{z})$ by applying Bayes' rule and marginalization. Thus, the remaining problem is to calculate the posterior pdfs $f(\boldsymbol{y}_k|\boldsymbol{z})$ for all $k \in \mathcal{K}$.

2.3. Joint Posterior Distribution and Factor Graph

The posterior pdf $f(\boldsymbol{x}_k, r_k|\boldsymbol{z}) = f(\boldsymbol{y}_k|\boldsymbol{z})$ is a marginal density of the joint posterior pdf $f(\boldsymbol{y}, \boldsymbol{y}^-, \boldsymbol{a}, \boldsymbol{b}|\boldsymbol{z})$. Under commonly made independence assumptions [1–3], one can show that [4]

$$f(\boldsymbol{y}, \boldsymbol{y}^-, \boldsymbol{a}, \boldsymbol{b}|\boldsymbol{z}) \propto \prod_{k=1}^{n_\mathrm{t}} f(\boldsymbol{y}_k|\boldsymbol{y}_k^-) f(\boldsymbol{y}_k^-|\boldsymbol{z}^-) \prod_{s=1}^{n_\mathrm{s}} \upsilon_s\big(\boldsymbol{y}_k, a_k^{(s)}; \boldsymbol{z}^{(s)}\big) \times \prod_{m=1}^{n_\mathrm{m}^{(s)}} \Psi_{km}^{(s)}\big(a_k^{(s)}, b_m^{(s)}\big). \quad (1)$$

Here $f(\boldsymbol{y}_k^-|\boldsymbol{z}^-)$ is the posterior pdf of $\boldsymbol{y}_k^-$, which was calculated at the previous time step, and $\upsilon_s\big(\boldsymbol{y}_k, a_k^{(s)}; \boldsymbol{z}^{(s)}\big)$ is a function involving the likelihood function $f\big(\boldsymbol{z}_m^{(s)}\big|\boldsymbol{x}_k\big)$ for $m = a_k^{(s)}$ [3, 4]. The factorization (1) can be represented by the factor graph [13] shown in Fig. 1, and an efficient and scalable approximate implementation of the marginalization operations converting $f(\boldsymbol{y}, \boldsymbol{y}^-, \boldsymbol{a}, \boldsymbol{b}|\boldsymbol{z})$ into the n_t marginal posterior pdfs $f(\boldsymbol{y}_k|\boldsymbol{z})$, $k \in \mathcal{K}$ can be obtained by employing the iterative SPA on this factor graph. To reduce the complexity and limit negative effects of loops in the factor graph, we use a message calculation schedule where *iterative* message passing is only performed for probabilistic data association, but not across the sensors [4]. Furthermore, in order to accommodate nonlinear/non-Gaussian state-transition and measurement models, we represent messages related to continuous state variables by particles [4]. Explicit expressions of the resulting messages and beliefs are provided in [3, 4] and will not be repeated here.

2.4. Extension to Multiple Dynamic Models

So far, the evolution of PT k was characterized by a single dynamic model (DM) described by $f(\boldsymbol{y}_k|\boldsymbol{y}_k^-)$. However, many tracking scenarios, such as those of maneuvering targets [19], require the use of different DMs in different time periods. Therefore, following the interacting multiple model approach [19, Ch. 11], we now model the evolution of the state of an existing PT $k \in \mathcal{K}$ as

$$\boldsymbol{x}_k = \boldsymbol{\xi}_{\ell_k}\big(\boldsymbol{x}_k^-, \boldsymbol{u}_k^{(\ell_k)}\big).$$

Here, $\boldsymbol{\xi}_{\ell_k}(\cdot, \cdot)$ is the state-transition function of PT k that is in force at the current time and $\boldsymbol{u}_k^{(\ell_k)}$ is a driving process that is assumed independent and identically distributed (iid) across time and k [1, 19]. The DM $\mathcal{D}_{\ell_k}$ is then defined by $\boldsymbol{\xi}_{\ell_k}(\cdot, \cdot)$ and the statistics of $\boldsymbol{u}_k^{(\ell_k)}$, and it is selected from a set $\{\mathcal{D}_j\}_{j=1}^J$ of possible DMs by the DM index $\ell_k \in \mathcal{J} \triangleq \{1, 2, \ldots, J\}$. From $\mathcal{D}_j$, one can obtain the state-transition pdf $f_j(\boldsymbol{x}_k|\boldsymbol{x}_k^-)$. The DM indices ℓ_k are modeled as discrete random variables that are independent across k and evolve according to a Markov chain with transition matrix $\boldsymbol{L} \in [0, 1]^{J \times J}$ [16]. That is, the transition probability mass function (pmf) of ℓ_k is given by $p(\ell_k = j|\ell_k^- = i) = [\boldsymbol{L}]_{i,j}$ for $i, j \in \mathcal{J}$.

Let us extend the augmented state $\boldsymbol{y}_k$ to include the DM index ℓ_k, i.e., we redefine it as $\boldsymbol{y}_k \triangleq [\boldsymbol{x}_k^\mathrm{T} \;\; r_k \;\; \ell_k]^\mathrm{T}$. Then, the DM $\mathcal{D}_j$ together with a suitable birth/death model implies the augmented state-transition pdf $f_j(\boldsymbol{y}_k|\boldsymbol{y}_k^-)$. We can now run the SPA on a factor graph that is equal to that in Fig. 1 except for the new definition of the variable nodes "$\boldsymbol{y}_k$" and "$\boldsymbol{y}_k^-$". This results in a multisensor MTT algorithm that automatically adapts its DM in each time step [16]. We note that this "multiple DM" formalism will also be used in Section 4 for the integration of geographic information.

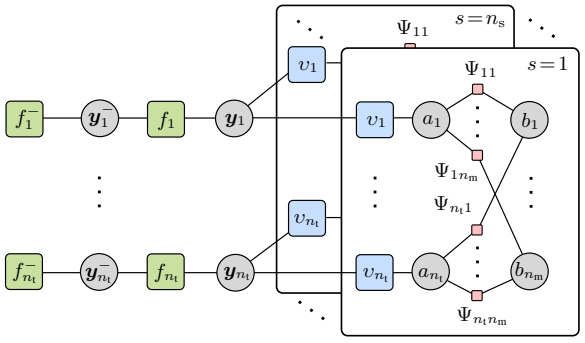

Fig. 1. Factor graph describing the factorization of $f(\boldsymbol{y}, \boldsymbol{y}^-, \boldsymbol{a}, \boldsymbol{b}|\boldsymbol{z})$ in (1). For simplicity, the sensor index s is omitted, and the following short notations are used: $f_k^- \triangleq f(\boldsymbol{y}_k^-|\boldsymbol{z}^-)$, $f_k \triangleq f(\boldsymbol{y}_k|\boldsymbol{y}_k^-)$, $\upsilon_k \triangleq \upsilon_s\big(\boldsymbol{y}_k, a_k^{(s)}; \boldsymbol{z}^{(s)}\big)$, and $\Psi_{km} \triangleq \Psi_{km}^{(s)}\big(a_k^{(s)}, b_m^{(s)}\big)$.

3. INTEGRATION OF AUXILIARY SURVEILLANCE DATA

In various applications, the MTT task is assisted by an auxiliary surveillance system, such as the automatic dependent surveillance broadcast (ADS-B) system in air traffic control [20] and the automatic identification system (AIS) system in maritime traffic control [14]. These systems are based on cooperative targets that autonomously broadcast reports informing about their current state. However, the fusion of this information is often difficult due to the asynchronicity and sparsity of these reports. Although each report usually includes a unique identification (ID), the association between targets and reports is not trivial: the ID may be absent, or it may be mistaken for a different ID, or it may be observed for the first time, in which case no prior information about the target is available.

Let us reconsider the multisensor MTT scenario from Section 2.1, with n_t PTs $k \in \mathcal{K}$ and n_s sensors $s \in \{1, 2, \ldots, n_\mathrm{s}\}$ produc-

ing measurements $\boldsymbol{z}_m^{(s)}$, $m \in \mathcal{M}^{(s)}$. We formally associate the reports from the auxiliary surveillance system with an additional sensor $s = 0$, and accordingly denote the reports as $\boldsymbol{z}_m^{(0)}$, $m \in \mathcal{M}^{(0)} \triangleq \{1, 2, \ldots, n_{\mathrm{m}}^{(0)}\}$. We assume that a target provides at most one report within one time step. Moreover, we assume that targets do not intentionally alter their reports, from which it follows that a report cannot be a false alarm. Therefore, the data association assumption for reports is phrased such that an existing PT can be associated with at most one report and a report is necessarily associated with an existing PT. The mth report $\boldsymbol{z}_m^{(0)}$ consists of state information $\boldsymbol{d}_m$ and ID ζ_m, i.e., $\boldsymbol{z}_m^{(0)} = [\boldsymbol{d}_m^{\mathrm{T}} \ \zeta_m]^{\mathrm{T}}$. Here, $\zeta_m \in \mathcal{L} \triangleq \{0, 1, \ldots, L\}$, where $\zeta_m \in \{1, 2, \ldots, L\}$ represents an ID identifying a target and $\zeta_m = 0$ represents the case in which the ID is absent. Furthermore, for each PT $k \in \mathcal{K}$, we introduce an ID label $\tau_k \in \mathcal{L}$, where $\tau_k = l \in \{1, 2, \ldots, L\}$ means that PT k produces reports with ID l, and $\tau_k = 0$ means that PT k produces reports without an ID. Finally, we redefine the augmented state vector to include the ID label, i.e., $\boldsymbol{y}_k \triangleq [\boldsymbol{x}_k^{\mathrm{T}} \ r_k \ \tau_k]^{\mathrm{T}}$, and the association vectors $\boldsymbol{a}$ and $\boldsymbol{b}$ to include $a_k^{(0)} \in \{0, 1, \ldots, n_{\mathrm{m}}^{(0)}\}$, $k \in \mathcal{K}$ and $b_m^{(0)} \in \{1, 2, \ldots, n_{\mathrm{t}}\}$, $m \in \mathcal{M}^{(0)}$, respectively.

Then, one can show that $f(\boldsymbol{y}, \boldsymbol{y}^-, \boldsymbol{a}, \boldsymbol{b}|\boldsymbol{z})$ factorizes as in (1), however with an additional factor corresponding to the additional sensor $s = 0$ [21]. That is, the product $\prod_{s=1}^{n_{\mathrm{s}}}$ in (1) is replaced by $\prod_{s=0}^{n_{\mathrm{s}}}$, which additionally involves the indicator factor $\Psi_{km}^{(0)}\big(a_k^{(0)}, b_m^{(0)}\big)$ and the report-related factor $\upsilon_0(\boldsymbol{y}_k, a_k^{(0)}; \boldsymbol{z}^{(0)})$. The factor $\Psi_{km}^{(0)}\big(a_k^{(0)}, b_m^{(0)}\big)$ additionally takes into account the no-false-alarm assumption (i.e., $b_m^{(0)}$ cannot be zero) and is therefore defined to be zero if and only if either $a_k^{(0)} = m$ and $b_m^{(0)} \neq k$ or $a_k^{(0)} \neq m$ and $b_m^{(0)} = k$ or $b_m^{(0)} = 0$, and one otherwise. The factor $\upsilon_0(\boldsymbol{y}_k, a_k^{(0)}; \boldsymbol{z}^{(0)})$ involves the likelihood function $f\big(\boldsymbol{z}_m^{(0)}\big|\boldsymbol{x}_k, \tau_k\big)$ for $m = a_k^{(0)}$. This likelihood function describes the asynchronous measurement model of the auxiliary surveillance system, including the statistical dependence of ζ_m and τ_k (see [21] for details). A scalable approximate calculation of the marginal posterior pdfs $f(\boldsymbol{x}_k, r_k, \tau_k|\boldsymbol{z})$ can now again be obtained by running the iterative SPA on the factor graph representing the factorization of $f(\boldsymbol{y}, \boldsymbol{y}^-, \boldsymbol{a}, \boldsymbol{b}|\boldsymbol{z})$. The resulting approximation of $f(\boldsymbol{x}_k, r_k, \tau_k|\boldsymbol{z})$ is used (after marginalizing out τ_k) for target detection and state estimation as explained in Section 2.2.

4. INTEGRATION OF GEOGRAPHIC INFORMATION

The performance of an MTT algorithm can be further improved by integrating geographic information about standard target routes, such as known sea lanes in a maritime scenario or known roads in a terrestrial scenario [15]. This type of information fusion can be accomplished by using the "multiple DM" formalism of Section 2.4 with suitable modifications. Consider J_{R} target routes indexed by $j \in \{1, 2, \ldots, J_{\mathrm{R}}\}$. We describe the movement of a PT along the jth route by a DM $\mathcal{D}_j$ as in Section 2.4, however with a directional driving process whose standard deviation in the direction orthogonal to the route is smaller than that in the direction of the route [22]. On the other hand, a PT may also move more irregularly off the standard routes (e.g., a ship during fishing operations); we describe this case by a DM $\mathcal{D}_0$ with a nondirectional driving process whose standard deviation is equal in all directions. Similarly to Section 2.4, we use a discrete random variable $\ell_k \in \{0, 1, \ldots, J_{\mathrm{R}}\}$ to select the DM index j that is in force for PT k at the current time; this DM is associated either with one of the J_{R} target routes ($\ell_k \in \{1, 2, \ldots, J_{\mathrm{R}}\}$) or with free movement ($\ell_k = 0$).

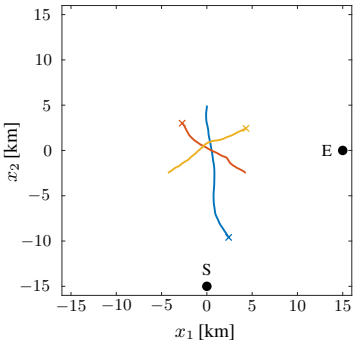

Fig. 2. Positions of the radar sensors (E, S) and exemplary realizations of the target trajectories. The crosses mark the final positions of the targets.

The evolution of ℓ_k is again modeled by a Markov chain. However, because the number of target routes J_{R} can be very large, we use a reduced Markov chain corresponding to a *variable structure interacting multiple model* [22]. The idea is to consider index transitions only to those target routes that are currently close enough so that they can be reached by the respective PT k. The set of these target route indices j depends on the PT index k and the previous PT state $\boldsymbol{x}_k^-$, and thus also the transition matrix $\boldsymbol{L}_k(\boldsymbol{x}_k^-)$ depends on k and on $\boldsymbol{x}_k^-$. Nonetheless, the reduced Markov chain is still consistent with the adaptive multi-DM formulation in Section 2.4, and thus the iterative SPA can be used as described there. This results in a multisensor MTT algorithm that automatically takes into account the knowledge of standard target routes. The fact that only a subset of all the DM index transitions is allowed typically leads to a significant reduction of complexity and also an improved tracking accuracy. A difference from Section 2.4 is the fact that the possible index transitions and the corresponding transition matrix $\boldsymbol{L}_k(\boldsymbol{x}_k^-)$ have to be determined at each time step and for each PT k.

5. SIMULATION RESULTS

We show simulation results demonstrating the fusion of measurements produced by two radar sensors and data provided by an auxiliary surveillance system as described in Section 3. Three targets move during 300 time steps in a square region-of-interest given by $[-15\,\mathrm{km}, 15\,\mathrm{km}] \times [-15\,\mathrm{km}, 15\,\mathrm{km}]$. The PT states consist of two-dimensional position and velocity, i.e., $\boldsymbol{x}_k = [x_{1,k} \ x_{2,k} \ \dot{x}_{1,k} \ \dot{x}_{2,k}]^{\mathrm{T}}$. Their evolution is governed by a single DM of the nearly-constant velocity type, i.e., $\boldsymbol{x}_k = \boldsymbol{A}\boldsymbol{x}_k^- + \boldsymbol{W}\boldsymbol{u}_k$, where the matrices $\boldsymbol{A} \in \mathbb{R}^{4\times4}$ and $\boldsymbol{W} \in \mathbb{R}^{4\times2}$ are chosen as in [19, Sec. 6.3.2] (with a time step duration of 10 seconds) and the driving process $\boldsymbol{u}_k \in \mathbb{R}^2$ is iid zero-mean Gaussian with a per-component standard deviation of $0.05\,\mathrm{m/s}^2$. (Extensions to multiple DMs can be easily obtained following the discussion in Section 2.4.) The targets exist at all times, and their trajectories are randomly generated in each simulation run. There are $n_{\mathrm{s}} = 2$ radar sensors, dubbed "S" and "E," which measure the targets' range and bearing. These range and bearing measurements are affected by Gaussian noise with standard deviation 100 m and 0.5°, respectively. The probability of detection is $q^{(1)} = q^{(2)} = 0.8$. The false-alarm pdf is chosen uniform on the region-of-interest; the number of false-alarm measurements is Poisson distributed with mean 2. Fig. 2 shows the positions of the two sensors and exemplary realizations of the three target trajectories.

The auxiliary surveillance data consist of the noisy positions (in Cartesian coordinates) and IDs of the three targets. The reported

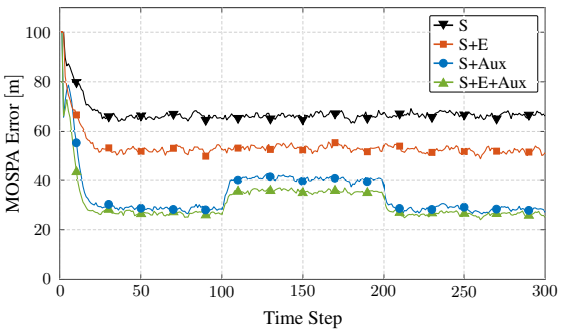

Fig. 3. MOSPA error obtained for different fusion strategies.

target positions are affected by Gaussian noise with a per-coordinate standard deviation of 10 m. On average, each target nominally sends 0.5 reports per time step. However, one of the three targets does not send any reports between time steps 100 and 200.

We compare the performance of the following four fusion strategies for MTT: (i) using only the measurements of sensor S (this strategy is referred to as *S*); (ii) fusing the measurements of the two sensors (*S+E*); (iii) fusing the measurements of sensor S and the auxiliary surveillance data (*S+Aux*); and (iv) fusing the measurements of the two sensors and the auxiliary surveillance data (*S+E+Aux*). For these strategies, Fig. 3 shows the Euclidean distance based mean optimal sub-pattern assignment (MOSPA) error with order $p = 1$ and cutoff parameter $c = 100$ m [23], averaged over 200 simulation runs and displayed versus time. The MOSPA error metric takes into account both the estimation errors for correctly detected targets and the errors due to incorrect target detections. The results in Fig. 3 clearly show the benefit of fusing the information from several sources. In particular, it is interesting that S+Aux consistently outperforms S+E, despite the asynchronous and intermittent nature of the auxiliary surveillance data. This superiority of S+Aux over S+E remains true even during the temporary absence of reports from one of the targets (which is indicated by an increased MOSPA error between time steps 100 and 200).

Table 1 compares the time-on-target (ToT) and the track fragmentation (TF), averaged over the three targets, for the four fusion strategies. The ToT is the fraction of time that a target is successfully tracked in the sense that the Euclidean distance between its estimated and true state is smaller than the MOSPA cutoff parameter $c = 100$ m. The TF is the number of subtracks associated with a target throughout its lifetime. Our ToT and TF results confirm the results in Fig. 3.

6. EXPERIMENTAL RESULTS USING REAL DATA

Finally, we present results of a numerical experiment based on real high-frequency surface wave (HFSW) radar measurements and real AIS data. The radar measurements were obtained by two Wellen Radar (WERA) systems [24] located on the coast of the Ligurian

Fusion Strategy	ToT	TF
S	74.5%	26.2
S+E	91.3%	13.3
S+Aux	95.4%	6.5
S+E+Aux	98.0%	3.8

Table 1. Average ToT and TF.

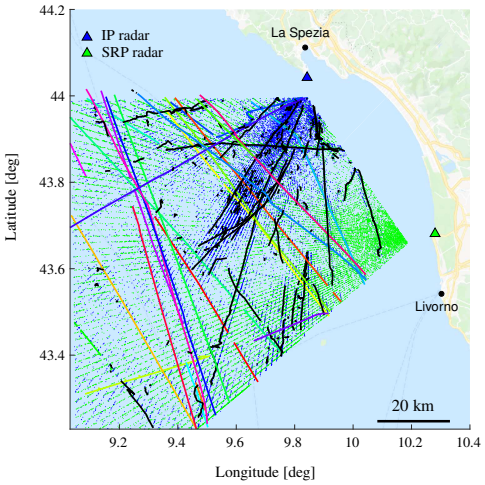

Fig. 4. Experimental results based on real data. Colored lines represent estimated trajectories corresponding to identified ships, while black lines represent estimated trajectories corresponding to false tracks or to ships not sending AIS data. Blue and green dots indicate the measurements of the IP and SRP radars, which are located at the position of the blue and green triangle, respectively. (Map courtesy of Google)

Sea, one on the island of Palmaria (IP) and the other in San Rossore Park (SRP). The radar measurements were produced by a 3D order statistics constant false alarm rate algorithm [17, Sec. 16.6]. Each measurement $\mathbf{z}_m^{(s)}$, $s \in \{1, 2\}$ consists of range, bearing, and range rate. The false-alarm pdf is chosen uniform on the surveillance region, which is the intersection of the fields-of-view of the two radar sensors; the number of false-alarm measurements is modeled by a Poisson distribution with mean 100.

Fig. 4 shows results obtained with the MTT algorithm described in Section 3, which fuses measurements of the two HFSW radars with AIS data. The figure distinguishes graphically between estimated trajectories where a nonzero ID label, i.e., a specific ship identity, has been detected and those that are false tracks or correspond to nonidentified ships (i.e., ships that do not send any AIS data). One can conclude from Fig. 4 that the fusion of radar measurements with AIS data is beneficial in that it enables ship identification for many of the estimated trajectories and, at the same time, it also allows the detection and tracking of ships that are not sending AIS data. Further results demonstrating the performance of the MTT algorithm with radar/AIS fusion are provided in [21].

7. CONCLUSION

The recently proposed sum-product algorithm (SPA) framework for multisensor-multitarget tracking constitutes a powerful and flexible basis for Bayesian information fusion. In this paper, we developed the fusion of multisensor radar measurements with data provided by an auxiliary surveillance system and with geographic information about standard target routes. This fusion was achieved by the formal inclusion of an additional sensor in the first case and by the introduction of multiple dynamic models in the second case. Experimental results using both simulated and real data demonstrated the effectiveness of our SPA-based fusion approach. Possible directions of future research include applications of the proposed framework to indoor localization [25, 26] and simultaneous localization and mapping [27, 28].

8. REFERENCES

[1] Y. Bar-Shalom, P. K. Willett, and X. Tian, *Tracking and Data Fusion: A Handbook of Algorithms*. Storrs, CT: Yaakov Bar-Shalom, 2011.

[2] R. P. S. Mahler, *Statistical Multisource-Multitarget Information Fusion*. Norwood, MA: Artech House, 2007.

[3] F. Meyer, T. Kropfreiter, J. L. Williams, R. A. Lau, F. Hlawatsch, P. Braca, and M. Z. Win, "Message passing algorithms for scalable multitarget tracking," *Proc. IEEE*, vol. 106, no. 2, pp. 221–259, Feb. 2018.

[4] F. Meyer, P. Braca, P. Willett, and F. Hlawatsch, "A scalable algorithm for tracking an unknown number of targets using multiple sensors," *IEEE Trans. Signal Process.*, vol. 65, no. 13, pp. 3478–3493, Jul. 2017.

[5] J. Williams and R. Lau, "Approximate evaluation of marginal association probabilities with belief propagation," *IEEE Trans. Aerosp. Electron. Syst.*, vol. 50, no. 4, pp. 2942–2959, Oct. 2014.

[6] J. Vermaak, S. J. Godsill, and P. Perez, "Monte Carlo filtering for multi target tracking and data association," *IEEE Trans. Aerosp. Electron. Syst.*, vol. 41, no. 1, pp. 309–332, Jan. 2005.

[7] B.-N. Vo, S. Singh, and A. Doucet, "Sequential Monte Carlo methods for multitarget filtering with random finite sets," *IEEE Trans. Aerosp. Electron. Syst.*, vol. 41, no. 4, pp. 1224–1245, Oct. 2005.

[8] B.-T. Vo, B.-N. Vo, and A. Cantoni, "Analytic implementations of the cardinalized probability hypothesis density filter," *IEEE Trans. Signal Process.*, vol. 55, no. 7, pp. 3553–3567, Jul. 2007.

[9] G. Battistelli, L. Chisci, S. Morrocchi, F. Papi, A. Farina, and A. Graziano, "Robust multisensor multitarget tracker with application to passive multistatic radar tracking," *IEEE Trans. Aerosp. Electron. Syst.*, vol. 48, no. 4, pp. 3450–3472, Oct. 2012.

[10] B.-N. Vo, B.-T. Vo, and D. Phung, "Labeled random finite sets and the Bayes multi-target tracking filter," *IEEE Trans. Signal Process.*, vol. 62, no. 24, pp. 6554–6567, Dec. 2014.

[11] J. L. Williams, "Marginal multi-Bernoulli filters: RFS derivation of MHT, JIPDA and association-based MeMBer," *IEEE Trans. Aerosp. Electron. Syst.*, vol. 51, no. 3, pp. 1664–1687, Jul. 2015.

[12] S. Nannuru, S. Blouin, M. Coates, and M. Rabbat, "Multisensor CPHD filter," *IEEE Trans. Aerosp. Electron. Syst.*, vol. 52, no. 4, pp. 1834–1854, Aug. 2016.

[13] F. R. Kschischang, B. J. Frey, and H.-A. Loeliger, "Factor graphs and the sum-product algorithm," *IEEE Trans. Inf. Theory*, vol. 47, no. 2, pp. 498–519, Feb. 2001.

[14] B. J. Tetreault, "Use of the automatic identification system (AIS) for maritime domain awareness (MDA)," in *Proc. MTS/IEEE OCEANS-05*, vol. 2, Washington, D.C., Sep. 2005, pp. 1590–1594.

[15] G. Pallotta, M. Vespe, and K. Bryan, "Vessel pattern knowledge discovery from AIS data: A framework for anomaly detection and route prediction," *Entropy*, vol. 15, no. 6, pp. 2218–2245, Jun. 2013.

[16] G. Soldi and P. Braca, "Online estimation of unknown parameters in multisensor-multitarget tracking: A belief propagation approach," in *Proc. FUSION-18*, Cambridge, UK, Jul. 2018, pp. 2151–2157.

[17] M. A. Richards, J. A. Scheer, and W. A. Holm, *Principles of Modern Radar: Basic Principles*. Raleigh, NC: Scitech Publishing, 2010.

[18] H. V. Poor, *An Introduction to Signal Detection and Estimation*, 2nd ed. New York, NY: Springer-Verlag, 1994.

[19] Y. Bar-Shalom, X. R. Li, and T. Kirubarajan, *Estimation with Applications to Tracking and Navigation*. New York, NY: Wiley, 2001.

[20] M. Strohmeier, M. Schafer, V. Lenders, and I. Martinovic, "Realities and challenges of NextGen air traffic management: The case of ADS-B," *IEEE Commun. Mag.*, vol. 52, no. 5, pp. 111–118, May 2014.

[21] D. Gaglione, P. Braca, and G. Soldi, "Belief propagation based AIS/radar data fusion for multi-target tracking," in *Proc. FUSION-18*, Cambridge, UK, Jul. 2018, pp. 2143–2150.

[22] G. Vivone, P. Braca, and J. Horstmann, "Knowledge-based multitarget ship tracking for HF surface wave radar systems," *IEEE Trans. Geosci. Remote Sens.*, vol. 53, no. 7, pp. 3931–3949, Jul. 2015.

[23] D. Schuhmacher, B.-T. Vo, and B.-N. Vo, "A consistent metric for performance evaluation of multi-object filters," *IEEE Trans. Signal Process.*, vol. 56, no. 8, pp. 3447–3457, Aug. 2008.

[24] K.-W. Gurgel, G. Antonischki, H.-H. Essen, and T. Schlick, "Wellen Radar (WERA): A new ground-wave HF radar for ocean remote sensing," *Coast. Eng.*, vol. 37, no. 3, pp. 219–234, Aug. 1999.

[25] M. Z. Win, F. Meyer, Z. Liu, W. Dai, S. Bartoletti, and A. Conti, "Efficient multi-sensor localization for the Internet-of-Things," *IEEE Signal Process. Mag.*, vol. 35, no. 5, pp. 153–167, Sep. 2018.

[26] K. Witrisal, P. Meissner, E. Leitinger, Y. Shen, C. Gustafson, F. Tufvesson, K. Haneda, D. Dardari, A. F. Molisch, A. Conti, and M. Z. Win, "High-accuracy localization for assisted living," *IEEE Signal Process. Mag.*, vol. 33, no. 2, pp. 59–70, Mar. 2016.

[27] E. Leitinger, F. Meyer, F. Hlawatsch, K. Witrisal, F. Tufvesson, and M. Z. Win, "A belief propagation algorithm for multipath-based SLAM," 2018, available online: http://arxiv.org/abs/1801.04463.

[28] E. Leitinger, S. Grebien, X. Li, F. Tufvesson, and K. Witrisal, "On the use of MPC amplitude information in radio signal based SLAM," in *Proc. IEEE SSP-18*, Freiburg, Germany, Jun. 2018, pp. 633–637.